

# Temperature Field Analysis and Optimization of the Homopolar Magnetic Bearing

Yu Cao\*, Chuang Liu, Shushu Zhu, and Junyue Yu

**Abstract**—The hybrid magnetic bearings (HMB) stabilize suspension in equilibrium position by providing bias flux through permanent magnets. The loss generated during operation causes the temperature of HMB to rise, which affects the stability of the magnetic bearing. In this paper, the loss and temperature of HMB are analyzed by finite element analysis software. The results show that the loss of HMB is mainly distributed in the rotor part, and the temperature of the rotor part is obviously higher than that of the stator part. The relationship between the structural parameters such as air gap length and pole width, and the loss of HMB is obtained by finite element analysis. According to the analysis results, the structural parameters are optimized by GAPS0. After optimization, the loss and temperature of HMB are significantly reduced.

## 1. INTRODUCTION

MB is a new type of high performance bearing that uses magnetic force to suspend the rotor in the air to achieve no mechanical contact between the rotor and stator. It has the advantages of no mechanical contact, no friction, no lubrication, long life, etc. [1–3]. It has been widely used in satellite attitude control [4], flywheel energy storage [5, 6], aerospace, high-speed machine tools [7], and vacuum ultra-clean. Compared with traditional bearings, magnetic bearing has many advantages, but its heating is a problem that cannot be ignored. Especially for the flywheel system supported by the magnetic suspension bearing, the working environment is high vacuum environment, and the heat dissipation condition is poor. The heat generated by loss will affect the normal operation of flywheel. So it is necessary to analyze the loss and temperature field when designing the magnetic bearing.

Many scholars have studied the loss and temperature field of magnetic bearings. In [8], Meeker and others have studied an analytical solution of rotor rotation loss including hysteresis loss and eddy current loss. The accuracy of the analytical solution is verified by comparing the experimental data. In [9], the loss of the bearing is studied, and the results show that the total loss of the hybrid radial magnetic bearing is higher than the total loss of the radial active magnetic bearing at the same speed. In [10], an analysis method based on magneto-resistive network method for calculating active magnetic bearing loss is proposed. This method can quickly estimate the loss of magnetic bearing and reduce development time and workload. In [11], the temperature field of radial magnetic bearings is analyzed by Ansys thermal analysis module. Considering the heat transfer mode of conduction and convection, the thermal analysis model of radial magnetic bearing is established, and the temperature field distribution of radial magnetic bearing is obtained. The temperature field distribution of the radial magnetic bearing is measured by infrared thermal imager. The experimental results are basically in agreement with the analysis results. In [12], a loss and temperature field calculation method considering electromagnetic coupling and temperature coupling is proposed, and two motors with a power system of 30 kW and a

---

*Received 28 July 2019, Accepted 4 September 2019, Scheduled 20 September 2019*

\* Corresponding author: Yu Cao (lx062200@126.com).

The authors are with the College of Electrical Engineering, Nanjing University of Aeronautics and Astronautics, Nanjing 211100, China.

rotational speed of 36000 r/pm are developed. The validity and accuracy of the method are verified. Although the loss and temperature of magnetic bearing are analyzed in the above literature, it has not been optimized.

In this paper, the loss and temperature distribution of hybrid magnetic bearings are studied, and the loss and temperature distribution of HMBs are obtained. Then the relationship between the loss of magnetic bearings and the structural parameters is analyzed. Finally, GAPSO optimization algorithm is used to optimize the design of hybrid magnetic bearings. Through optimization, the loss and temperature rise of hybrid magnetic bearings are significantly reduced, which improves the operation performance of magnetic bearings.

## 2. STRUCTURE AND LOSS ANALYSIS OF HMB

### 2.1. Structure and Parameters of HMB

The structure of the homopolar hybrid magnetic bearing studied in this paper is shown in Figure 1. The homopolar HMB provides a bias magnetic flux through the permanent magnet, and the rotor is stably suspended in the equilibrium position under the bias magnetic flux without external disturbance. When the rotor is disturbed, the control current is fed into the control coil to generate the control flux. The control flux and bias flux work together to stabilize the rotor suspension. The structure parameters of hybrid magnetic bearings are shown in Table 1.

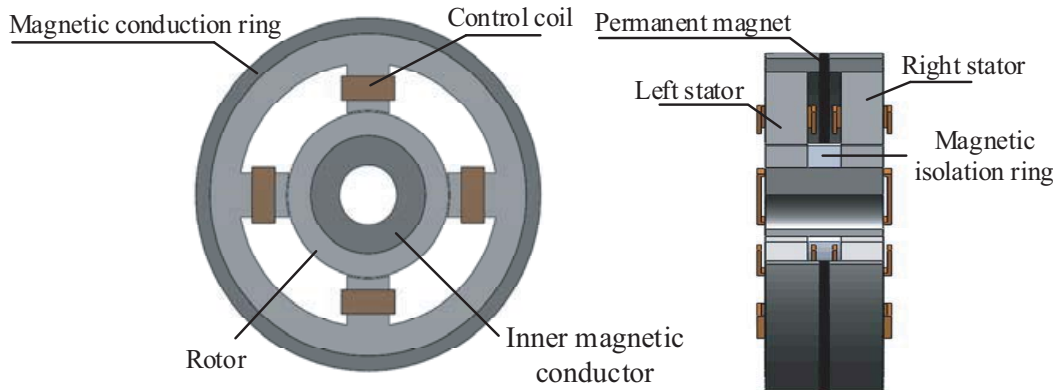


**Figure 1.** Structure of HMB.

**Table 1.** Structural parameters of HMB.

Parameter	value
outer diameter of stator/mm	120
inner diameter of stator/mm	90
inner diameter of Magnetic conduction ring/mm	110
outer diameter of rotor/mm	28
The axial length of left stator/mm	12
The axial length of right stator/mm	12
The length of permanent magnet/mm	2
The width of stator tooth/mm	14.3
Air gap length/mm	0.5
Turns of winding	60

## 2.2. Loss Analysis of HMB

The loss of HMB is the main cause of heating, so the loss of HMB should be analyzed before the temperature field analysis. HMB uses permanent magnet to provide bias flux, which effectively reduces excitation loss. Its loss mainly includes core loss, copper loss, and additional loss [13–16]. Because the additional loss is very small compared with copper loss and core loss, it can be neglected. Therefore, this paper mainly considers the copper loss and core loss of HMB.

### 2.2.1. Copper Loss

The copper loss of HMB is caused by the control current through the winding resistance when magnetic bearings are disturbed by the outside world. According to Ohm's law, the formula for calculating the copper loss is as follows

$$P_{\text{cu}} = i^2 R = i^2 N \frac{\rho_{\text{cu}} l}{A_{\text{cu}}} \quad (1)$$

where  $P_{\text{cu}}$  is the copper loss, and  $i$  is the current flowing through the control coil. For active magnetic bearing, copper current consumption is the sum of the bias current and control current, and for hybrid magnetic bearing, bias magnetic flux is provided by permanent magnets, so the current consumption for calculating copper is only the control current.  $R$  is the total resistance of the coil,  $\rho_{\text{cu}}$  the resistivity of the copper wire,  $A_{\text{cu}}$  the cross-sectional area of the copper wire,  $l$  the average length of the single-turn coil, and  $N$  the total number of turns of the coil.

### 2.2.2. Core Loss

The core loss of HMB is caused by the change of the magnitude and frequency of magnetic flux density, which is mainly located on the stator and rotor. When the rotor is stably suspended, no control current is applied to the control coil, and only the bias magnetic flux is present in the stator core. The generated core loss is small. For the rotor, the rotational speed is high during operation, and even if the control current is zero, the bias magnetic flux on the rotor and the change in the magnetic flux density  $B$  flowing in the air gap in the air gap cause core loss in the rotor.

The core loss is divided into hysteresis loss  $P_h$  and eddy current loss  $P_e$ , and the calculation formula is as follows

$$P_{\text{Fe}} = P_e + P_h = \frac{1}{6\rho} \pi^2 e^2 f_r^2 B_m^2 V_{\text{Fe}} \gamma_{\text{Fe}} + k_h f_r B_m^{1.6} V_{\text{Fe}} \gamma_{\text{Fe}} \quad (2)$$

where  $P_{\text{Fe}}$  is the core loss of the magnetic bearing,  $P_e$  the eddy current loss,  $P_h$  the hysteresis loss,  $\rho$  the unit resistance of the iron core,  $e$  the lamination thickness of the silicon steel sheet,  $f_r$  the re-magnetization frequency of the magnetic field in the air gap,  $B_m$  the magnitude of the alternating magnetic induction,  $V_{\text{Fe}}$  the volume of the core,  $\gamma_{\text{Fe}}$  the density of the core material, and  $k_h$  the hysteresis loss factor.

## 3. THERMAL MODEL AND TEMPERATURE FIELD ANALYSIS

### 3.1. Thermal Model

In this paper, the temperature field of magnetic bearings is analyzed by means of electromagnetic-thermal unidirectional coupling. Firstly, the thermal model of magnetic bearing is established. The HMB is composed of a stator, a rotor, coils, and a permanent magnet. In order to simplify the thermal model, the following points should be considered:

1. The ambient temperature of the HMB should be kept constant. The initial temperature of the magnetic bearing and the initial temperature of the material should be consistent with the ambient temperature.
2. Most of the heat generated by the rotor of magnetic bearings is dispersed through stator heat conduction and convective heat dissipation. Therefore, the temperature effect of the stator should be considered as a certain ambient temperature when simulating the temperature field.

3. The windings of magnetic bearings are treated as a heat conducting body. When the windings are equivalent, the volume of the windings before and after the equivalent is guaranteed to remain unchanged. All the insulation in the stator slot is insulated in the same slot, which is equivalent to a heat conducting body.
4. The average heat dissipation coefficients of stator outer surface and rotor end surface are obtained.

Based on the above considerations, the 3D finite element thermal analysis model of the equivalent HMB established in this paper is shown in Figure 2. The winding is equivalent to a heat conductor, and the winding copper wire paint film, impregnating varnish, and groove insulation are equivalent to another heat conductor. The air gap between the stator and rotor is equivalent to a cylindrical heat conductor.

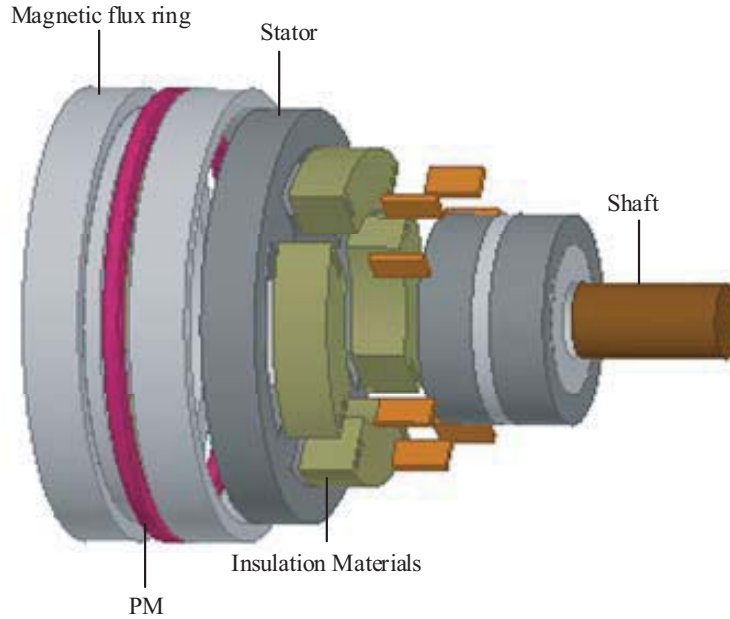


**Figure 2.** Equivalent thermal model.

### 3.2. Boundary Conditions and Thermal Parameters

Heat transfer is an extremely common process of energy transfer. Due to temperature difference, heat is transferred from a high temperature object to a low temperature object until temperature equilibrium is reached. According to the heat transfer mechanism, heat transfer is mainly divided into three types: heat conduction, heat convection, and heat radiation [17, 18].

The conduction of heat between objects due to the change of temperature gradient is heat conduction, which is the main way of heat transfer, and its expression is

$$Q = -\lambda S \frac{dT}{dn} \quad (3)$$

where  $Q$  is the heat flux ( $W$ ),  $\lambda$  the thermal conductivity of the material ( $W/(m \cdot ^\circ C)$ ),  $S$  the heat transfer area ( $m^2$ ) of the material, and  $\frac{dT}{dn}$  the temperature gradient ( $^\circ C/m$ ).

Thermal convection refers to the relative motion between the fluid with higher temperature and the fluid with lower temperature, which is caused by the existence of relative displacement and temperature difference. The process can be divided into natural convection and forced convection. Its expression is

$$Q = hS(t_s - t_r) \quad (4)$$

where  $h$  is the convective heat dissipation coefficient ( $W/(mm \cdot ^\circ C)$ ),  $t_s$  the material surface temperature ( $^\circ C$ ), and  $t_r$  the fluid temperature ( $^\circ C$ ).

Thermal radiation refers to the process by which an object transmits heat by emitting electromagnetic energy. Thermal radiation does not require any medium, and the heat radiation efficiency in vacuum is the highest. The heat transfer amount of the two radiation surfaces can be expressed as

$$\Phi_{1,2} = \frac{\sigma_b (T_1^4 - T_2^4)}{\frac{1 - \varepsilon_1}{\varepsilon_1 A_1} + \frac{1}{A_1 X_{1,2}} + \frac{1 - \varepsilon_2}{\varepsilon_2 A_2}} \quad (5)$$

where  $\Phi_{1,2}$  is the amount of heat transfer between radiating surfaces 1 and 2;  $\varepsilon_1, \varepsilon_2$  are the emissivity of radiating surfaces 1 and 2, and the value is between 0 and 1; and  $A_1, A_2$  are the surface area of radiating surfaces 1 and 2;  $X_{1,2}$  is the radiating surfaces 1 and 2. The angular coefficient (representing the ratio of the radiant energy emitted by surface 1 absorbed by surface 1 to the total radiant energy emitted by surface 2)  $\sigma_b$  is the blackbody radiation constant, and its value is  $5.67 \times 10^{-8}$ .  $T_1, T_2$  are the temperatures of radiating surfaces 1 and 2 [19].

When determining the thermal parameters of HMB, it is assumed that the thermal conductivity of each component material does not vary with temperature. The HMB winding is made of multiple enameled copper wires. In order to simplify the calculation, it is equivalent to a heat conducting body, and its equivalent thermal conductivity is calculated as follows

$$\lambda_{eq} = \lambda_{cu} F_{ew} + \lambda_{imp} (1 - F_{ew}) \quad (6)$$

where  $\lambda_{cu}$  is the thermal conductivity of copper,  $\lambda_{imp}$  the thermal conductivity of the insulating material, and  $F_{ew}$  the slot full rate. The thermal conductivity of each part of the material is shown in Table 2.

**Table 2.** Thermal parameters of materials.

Component	Density (kg/m <sup>3</sup> )	Specific heat capacity (J/kg · K)	Thermal Conductivity (W/(m · K))
Stator and rotor	7800	465	52
Insulation materials	1700	1340	0.326
Winding	8900	390	380
Shaft	7700	480	50.2
Permanent magnets	8300	540	10

### 3.3. Analysis of Simulation Results of Temperature Field

The Ansys workbench is used to analyze the transient magnetic-thermal coupling of HMB. The loss distribution of magnetic bearings with only bias flux is obtained by electromagnetic field analysis and calculation as shown in Figure 3. It can be seen from the figure that the loss of magnetic bearings mainly distributes in the rotor part when only the bias flux exists, and the loss of stator part is negligible.

The loss is applied as a heat source to the transient temperature field to obtain the magnetic bearing heat source distribution as shown in Figure 4. It can be seen from the figure that the heat source is mainly distributed in the rotor portion.

The temperature distribution of each component of the HMB is obtained by analyzing the temperature field of the HMB as shown in Figure 5.

It can be seen from Figure 5 that when the HMB has only a bias magnetic flux, the temperature of the rotor is significantly higher than the stator. The stator of HMB has a very small loss when it is stably suspended. Its outer surface is close to the external environment; the heat dissipation area is large; and the heat dissipation condition is good, so the temperature is low. Due to the change in magnetic flux density in the air gap, the loss on the stator teeth is greater than the loss on the stator yoke, and the temperature rise is large. When the rotor is in a stable suspension state, the eddy current loss induced by the change of the magnetic flux density  $B$  is large due to high rotation speed, and the heat dissipation condition of rotor is poor, so the temperature is high.

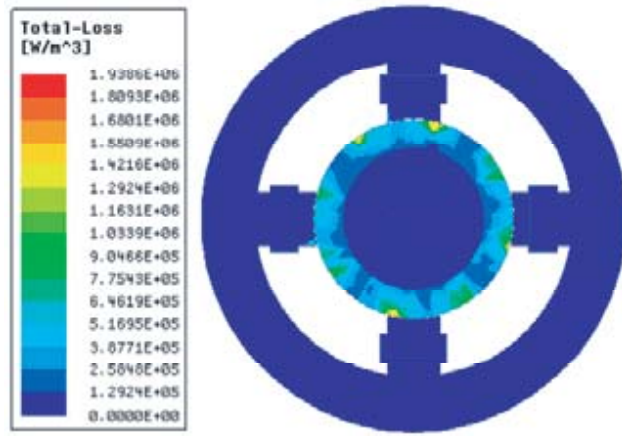


Figure 3. Loss distribution map of HMB.

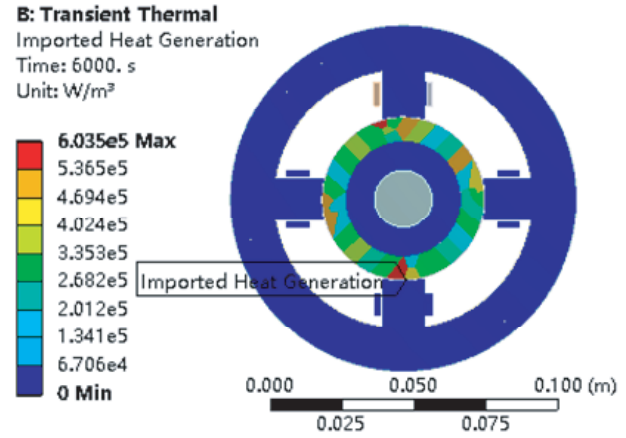
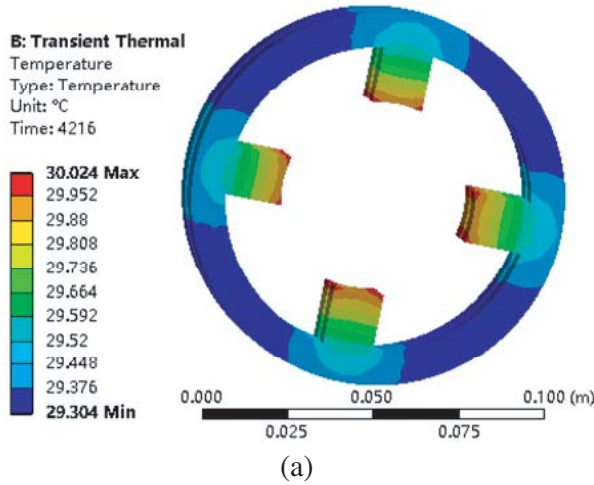
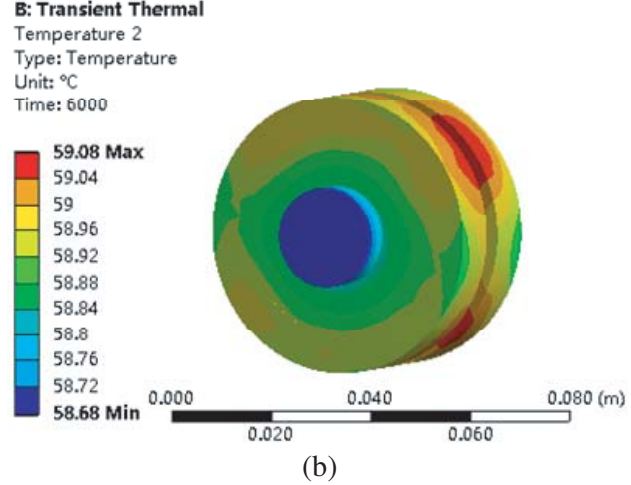


Figure 4. Heat source distribution diagram of HMB.



(a)



(b)

Figure 5. Temperature distribution of various components of the magnetic bearing. (a) Stator temperature. (b) Rotor temperature.

## 4. OPTIMIZATION DESIGN OF HMB

### 4.1. Influence of Structural Parameters of HMB on Core Loss

It can be obtained from Eq. (2) that the larger the magnitude of the magnetic flux density  $B$  is, the faster the magnetization frequency is, and the greater the core loss is. The change of the HMB speed, air gap length, and stator pole width affects magnetic flux density amplitude  $B$  and re-magnetization frequency, resulting in a change in core loss. This paper will study the relationship among air gap length, pole width, and loss.

#### 4.1.1. Influence of Air Gap Length on Core Loss of HMB

According to the parameters in Table 1, the finite element simulation model of HMB is established. When the rotor speed is 30000 r/min, the relationship between core loss and air gap length of HMB is shown in Figure 6. It can be seen from the figure that with the increase of air gap length, the core loss of HMB decreases gradually.

As the length of air gap increases, the air gap magnetoresistance increases; the flux density

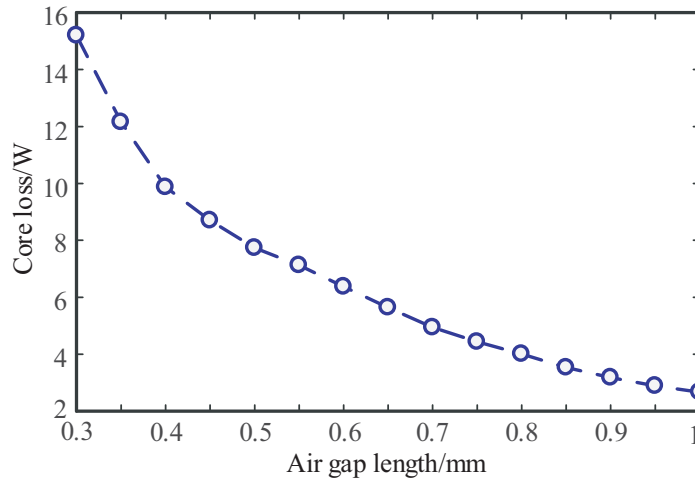


**Figure 6.** Relationship between core loss and air gap length.

decreases; and the suspension force decreases. In order to ensure that HMB can provide sufficient suspension force, the length of permanent magnets must be increased. When the air gap length is 0.8 mm, the loss of HMB is very small, but the consumption of permanent magnets is greatly increased. According to the above analysis, the air gap length should be between 0.3 mm and 0.8 mm.

4.1.2. Influence of Pole Width on Core Loss of HMB

The core losses of HMB with different pole widths are obtained by finite element simulation as shown in Table 3.

**Table 3.** Relationship between pole width and core loss.

Pole width /mm	Core loss/W	Error
14.7	9.33	0
15.7	8.9	-4.6%
16.6	8.67	-2.5%
17.6	8.52	-1.7%

It can be obtained from the table that as the width of the pole increases, the core loss gradually decreases. Due to the increase in the width of the pole, the amplitude fluctuation of the magnetic flux density in the rotor core is reduced, and the core loss is reduced. Therefore, on the basis of ensuring the comprehensive performance of the HMB, the width of the pole should be appropriately increased to reduce the core loss.

4.2. Optimization of Structural Parameters

Through the above analysis, the relationship between the core loss of the HMB and various parameters is obtained. In order to reduce the core loss and temperature rise, structural parameters of the HMB are optimized in this section.

Optimizing objective: Volume  $V$  and core loss  $P_{Fe}$  of HMB. The volume calculation formula is

$$V = V_r + V_{ls} + V_{pm} + V_{rs} \tag{7}$$

where  $V_r$  is the volume of the rotor,  $V_{ls}$  the volume of the stator on the left side,  $V_{pm}$  the volume of the permanent magnet, and  $V_{rs}$  the volume of the stator on the right side.

**Table 4.** Design parameters and scope.

Parameter	variables	Ranges
outer diameter of stator/mm	$d_6$	(100, 120)
outer diameter of rotor/mm	$d_2$	(25, 30)
Axial length/mm	$l$	(35, 45)
Permanent magnet thickness/mm	$l_{pm}$	(1.5, 2.5)
Pole Width/mm	$d_0$	(8.65, 19.8)
Air gap length /mm	$g$	(0.3, 0.8)

**Optimizing variables:** The design variables and the range of values of HMB are shown in Table 4.

**Constraint:** In order to ensure that the rotor can be stably suspended in the equilibrium position and avoid soft magnetic material saturation, the suspension force  $F$  and air gap flux density  $B$  should satisfy

$$\begin{cases} F \geq 120 \text{ N} \\ 0.4 \text{ T} \leq B \leq 0.6 \text{ T} \end{cases} \quad (8)$$

### 4.3. Analysis of Optimization Results

Parameters of the HMB before and after optimization are shown in Table 5.

According to the optimized parameters, the thermal analysis model of the HMB is established, and the temperature distribution is shown in Figure 7.

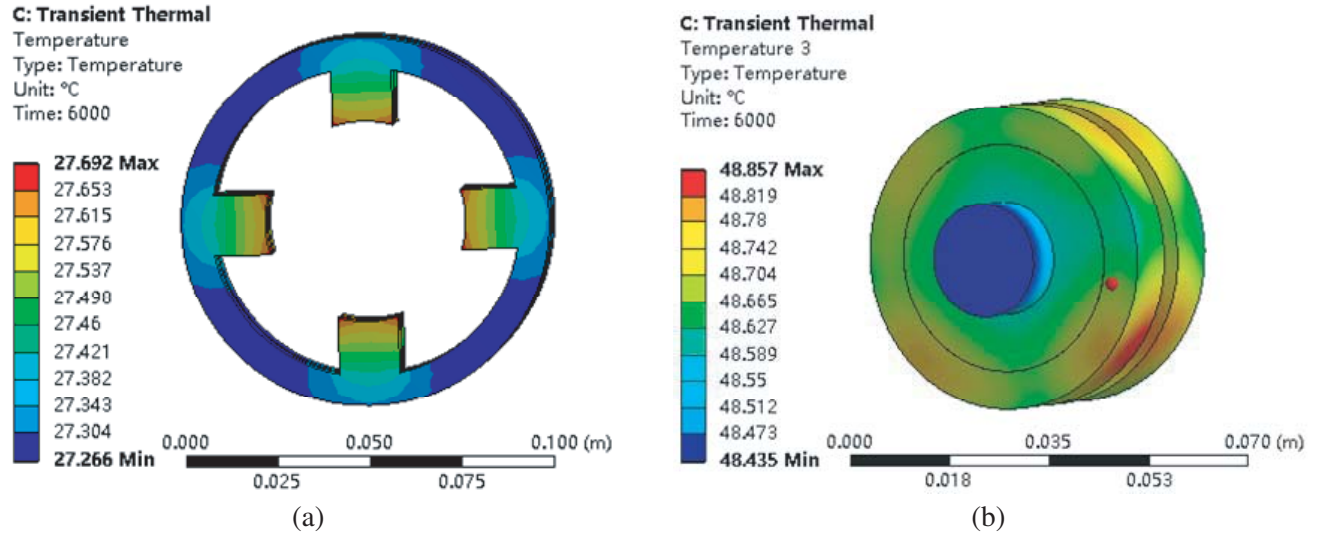


**Figure 7.** Temperature distribution of Optimized HMB. (a) Stator temperature. (b) Rotor temperature.

It can be seen from the figure that the temperature of each component of the hybrid magnetic bearing is significantly reduced, wherein the temperature of the stator is lowered by 3°C, and the temperature of the rotor is reduced by about 10°C. The reduction of the temperature of the HMB can effectively improve the stability of the magnetic bearing operation.

**Table 5.** Results before and after optimization.

Parameter	Initial value	Optimized value
$d_6/\text{mm}$	120	112
$d_5/\text{mm}$	110	100
$d_2/\text{mm}$	28	26.7
$g_0/\text{mm}$	0.5	0.6
$l_{pm}/\text{mm}$	2	2
$l/\text{mm}$	12	10
$d_0/\text{mm}$	14.75	16.42
$F/N$	130	132
$V/\text{m}^3$	1.80E-4	1.35E-4
$P/W$	11.85	7.86

## 5. CONCLUSIONS

In this paper, HMB is taken as the research object, and its loss and temperature are analyzed by finite element analysis software. The simulation results show that: (1) the loss of HMB is mainly distributed in the rotor part under high-speed operation; (2) the temperature of the hybrid magnetic bearing rotor is significantly higher than the stator temperature. The relationship between structural parameters such as air gap length, pole width, and loss is obtained by finite element analysis. According to the analysis results, the structural parameters of HMB are optimized by GAPS0 optimization algorithm. After optimization, the loss and temperature are significantly reduced compared with that before optimization.

## REFERENCES

1. Eryong, H. and L. Kun, "A novel structure for low loss radial hybrid magnetic bearing," *IEEE Transactions on Magnetics*, Vol. 47, No. 12, 4725–4733, 2011.
2. Santra, T., D. Roy, and A. B. Choudhury, "Calculation of passive magnetic force in a radial magnetic bearing using general division approach," *Progress In Electromagnetics Research M*, Vol. 54, 91–102, 2017.
3. Yuan, Y., Y. K. Sun, Q. W. Xiang, et al., "Model-free adaptive control for three-degree-of-freedom hybrid magnetic bearings," *Frontiers of Information Technology & Electronic Engineering*, Vol. 18, No. 12, 2035–2045, 2017.
4. Sun, J., Y. Ren, and J. Fang, "Passive axial magnetic bearing with Halbach magnetized array in magnetically suspended control moment gyro application," *Journal of Magnetism and Magnetic Materials*, Vol. 323, No. 15, 2103–2107, 2011.
5. Han, B., S. Zheng, X. Wang, and Y. Qian, "Integral design and analysis of passive magnetic bearing and active radial magnetic bearing for agile satellite application," *IEEE Transactions on Magnetics*, Vol. 48, No. 6, 1959–1966, 2012.
6. Nguyen, T. D. and G. Foo, "Sensorless control of a dual-airgap axial flux permanent magnet machine for flywheel energy storage system," *IET Electric Power Applications*, Vol. 7, No. 2, 140–149, 2013.
7. Knospe, C. R., "Active magnetic bearings for machining applications," *Control Engineering Practice*, Vol. 15, No. 3, 307–313, 2007.
8. Meeker, D. C., A. V. Filatov, and E. H. Maslen, "Effect of magnetic hysteresis on rotational losses in heteropolar magnetic bearings," *IEEE Transactions on Magnetics*, Vol. 40, No. 3, 3302–3307, 2004.

9. Bakay, L., M. Dubois, P. Viarouge, et al., "Losses in hybrid and active magnetic bearings applied to Long Term Flywheel Energy Storage," *IET International Conference on Power Electronics*, IET, 2010.
10. Chong, L., R. Dutta, M. F. Rahman, et al., "Experimental verification of core and magnet losses in a concentrated wound IPM machine with V-shaped magnets used in field weakening applications," *Electric Machines & Drives Conference*, IEEE, 2011.
11. Romanenko, A., A. Smirnov, R. P. Jastrzebski, et al., "Losses estimation and modelling in active magnetic bearings," *European Conference on Power Electronics & Applications*, 2014.
12. Xin, L. and C. Wu, "Analysis and calculation of temperature field of radial magnetic bearing," *Machinery*, Vol. 49, No. 4, 18–21, 2011.
13. Ren, X., Y. Le, B. Han, and K. Wang, "Loss and thermal estimation method of a magnetic bearing system considering electromagnetic and temperature coupling," *International Conference on Electrical Machines & Systems*, IEEE, 2017.
14. Shelke, S. and R. V. Chalam, "Optimum energy loss in electromagnetic bearing," *Proceedings of the IEEE*, 3, 2011.
15. Zaki, M., O. Mahgoub, A. Adly, et al., "Three-dimensional finite element modeling of active magnetic bearings considering eddy current losses in laminated rotor," *IEEE Magnetics Conference*, 2015.
16. Bakay, L., M. Dubois, P. Viarouge, et al., "Losses in an optimized 8-pole radial AMB for Long Term Flywheel Energy Storage," *International Conference on Electrical Machines & Systems*, IEEE, 2010.
17. Romanenko, A., A. Smirnov, R. P. Jastrzebski, and O. Pyrhonen, "Losses estimation and modelling in active magnetic bearings," *2014 16th European Conference on Power Electronics and Applications*, IEEE, 2014.
18. Abukhshim, N. A., P. T. Mativenga, and M. A. Sheikh, "Heat generation and temperature prediction in metal cutting: A review and implications for high speed machining," *International Journal of Machine Tools and Manufacture*, Vol. 46, Nos. 7–8, 782–800, 2006.
19. Jiang, W. Y. and T. M. Jahns, "Coupled electromagnetic-thermal analysis of electric machines including transient operation based on finite-element techniques," *IEEE Transactions on Industry Applications*, Vol. 51, No. 2, 1880–1889, 2015.